Development of Orally Bioavailable and CNS Penetrant Biphenylaminocyclopropane Carboxamide Bradykinin B_1 Receptor Antagonists

Scott D. Kuduk,*,† Christina N. Di Marco,† Ronald K. Chang,† Michael R. Wood,† Kathy M. Schirripa,† June J. Kim,† Jenny M. C. Wai,† Robert M. DiPardo,† Kathy L. Murphy,‡ Richard W. Ransom,‡ C. Meacham Harrell,‡ Duane R. Reiss,‡ Marie A. Holahan,‡ Jacquelynn Cook,‡ J. Fred Hess,‡ Nova Sain,§ Mark O. Urban,§ Cuyue Tang,|| Thomayant Prueksaritanont,|| Douglas J. Pettibone,‡ and Mark G. Bock†

Departments of Medicinal Chemistry, Neuroscience Drug Discovery, Pain Research, and Drug Metabolism, Merck Research Laboratories, Sumneytown Pike, P.O. Box 4, West Point, Pennsylvania 19486

Received September 19, 2006

A series of biphenylaminocyclopropane carboxamide based bradykinin B_1 receptor antagonists has been developed that possesses good pharmacokinetic properties and is CNS penetrant. Discovery that the replacement of the trifluoropropionamide in the lead structure with polyhaloacetamides, particularly a trifluoroacetamide, significantly reduced P-glycoprotein mediated efflux for the series proved essential. One of these novel bradykinin B_1 antagonists (**13b**) also exhibited suitable pharmacokinetic properties and efficient ex vivo receptor occupancy for further development as a novel approach for the treatment of pain and inflammation.

Introduction

It has been estimated that roughly 40 million Americans suffer from chronic pain as a result of ailments ranging from osteoarthritis and diabetic neuropathy to cancer pain. The societal cost as a result is significant with depression, anxiety, and insomnia as comorbidities. Accordingly, new and improved treatments for pain represent a prominent area of unmet medical needs.

Bradykinin peptides (kinins) are rapidly produced from high molecular weight kininogen precursor proteins following the activation of kallikrein enzymes after tissue injury.[1] Kinins produce a variety of physiological effects, most notably, pain and inflammation.[2] These effects are transduced by two distinct G-protein coupled receptors designated as B_1 and B_2.[3] The B_2 receptor is largely constitutively expressed in a number of tissues and evokes the acute pain response following activation by the kinin peptides bradykinin (Arg-Pro-Pro-Gly-Phe-Ser-Pro-Phe-Arg) and kallidin (Lys-Arg-Pro-Pro-Gly-Phe-Ser-Pro-Phe-Arg). Their corresponding metabolites, [des-Arg9]BK (DABK) and [des-Arg10]kallidin, serve as agonists for the B_1 receptor, which is induced following pro-inflammatory and painful stimuli and otherwise expressed at very low levels in healthy tissue.[4] These peptide agonists have been shown to produce hyperalgesia in animal models that can be successfully blocked by peptide derived B_1 antagonists.[5,6] In addition, B_1 receptor knockout mice have shown muted responses to thermal, chemical, and mechanical nociceptive stimuli, while appearing normal in all other respects.[7,8]

Many B_1 receptor mediated effects, including pain, involve peripheral mechanisms. The B_1 receptor is also constitutively expressed in the central nervous system (CNS) of rats and mice, suggesting a central component in pain perception.[9−11] This has been supported by the demonstration of a hypoalgesic response when B_1 antagonists were administered centrally.[12,13] Thus, CNS penetrant bradykinin B_1 receptor antagonists are of considerable interest as they may have superior efficacy relative to peripheral B_1 antagonists and might also find additional application in the treatment of neuropathic pain.

In the past several years, non-peptide, small molecule antagonists of the B_1 receptor have been reported.[14] For example, we have recently shown that 2,3-diaminopyridine bradykinin B_1 antagonists exhibit a high affinity for the human B_1 receptor, good pharmacokinetic properties, and in vivo efficacy in rabbit models of hyperalgesia and inflammation.[15,16] However, the 2,3-diaminopyridine core has proven to lead to high levels of bioactivation in vitro and in vivo, prohibiting further development of these compounds as clinical candidates.[17]

It was recently disclosed that α-amino cyclopropylamides can serve as effective surrogates for the 2,3-diaminopyridine nucleus.[18] Merging this new cyclopropylamide scaffold with the critical components of diaminopyridine **1** (the trifluoropropionamide and the B/C ring biphenyl) successfully led to biphenylaminocyclopropane carboxamides such as **2a** (Figure 1). While **2a** showed excellent human B_1 receptor binding affinity and promising pharmacokinetic properties, it also proved to be a significant substrate for human P-glycoprotein (P-gp) mediated efflux,[19] indicating that low levels of CNS penetration in man would be expected. In this paper, we report our efforts to decrease the P-gp mediated efflux of this cyclopropane carboxamide series with the goal of discovering a suitably CNS penetrant preclinical candidate for further development.

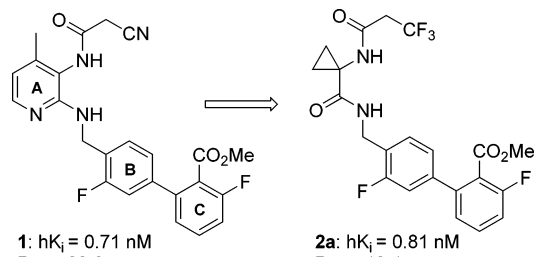

Figure 1. Genesis of lead structure **2**.

* To whom correspondence should be addressed. Tel.: (215) 652-5147; fax: (215) 652-3971; email: scott_d_kuduk@merck.com.
† Department of Medicinal Chemistry.
‡ Department of Neuroscience Drug Discovery.
§ Department of Pain Research.
|| Department of Drug Metabolism.

10.1021/jm061094b CCC: $37.00
Published on Web 12/23/2006

Scheme 1[a]

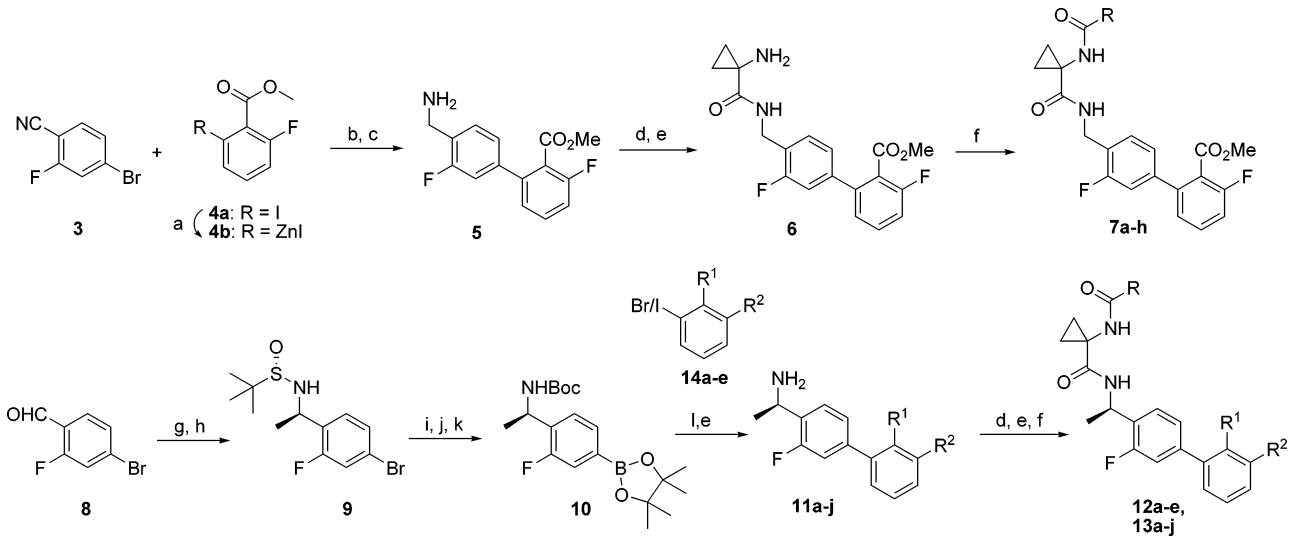

[a](a) Rieke Zn, THF, 60°C. (b) $Pd(Ph_3P)_4$, 60°C, THF. (c) RaNi, H_2, NH_3-MeOH. (d) 1-(*N*-*t*-Boc-amino)-cyclopropane carboxylic acid, EDC, TEA, HOBt, DMF. (e) HCl, EtOAc. (f) EDC, TEA, RCO_2H, HOBt, CH_2Cl_2. (g) (*S*)-*t*-butyl sulfinamide, CH_2Cl_2, $MgSO_4$. (h) MeMgBr, CH_2Cl_2, -48 °C. (i) HCl, dioxane. (j) Boc_2O, CH_2Cl_2. (k) pinacoldiboron ester, KOAc, DMSO, $Pd(dppf)Cl_2$. (l) $Pd(OAc)_2$, $(tol)_3P$, K_2CO_3, THF-H_2O, 80 °C.

Scheme 2[a]

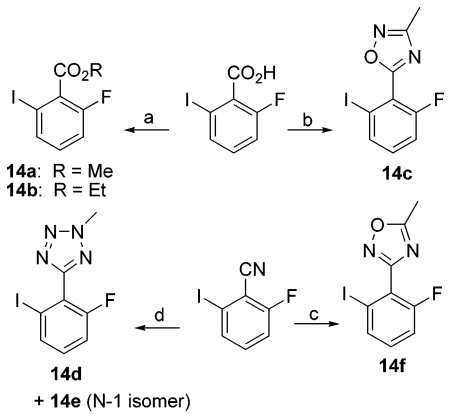

[a](a) K_2CO_3, DMF, MeI or EtI (b) i. oxalyl chloride, CH_2Cl_2, ii. NH_3, CH_2Cl_2, iii. dimethylacetamide dimethylacetal, 120 °C, iv. NH_2OH, AcOH. (c) i. NH_2OH, EtOH, 80 °C, ii. dimethylacetamide dimethylacetal, 120 °C. (d) i. Me_3SnN_3, toluene, 120 °C, ii. MeI, K_2CO_3, DMF.

Chemistry

Scheme 1 details the routes employed to access the biphenylaminocyclopropane carboxamides used in this study. Negishi cross coupling between bromide **3** and zinc reagent **4b** followed by nitrile reduction produced biphenylamine **5**. Coupling **5** with the Boc protected aminocyclopropane carboxylic acid and consequent deprotection afforded amine **6**. Acylation of amine **6** via EDC mediated coupling with the appropriate acid afforded compounds **7a**−**h**.

For compounds bearing a chiral center via the addition of a methyl group at the benzylic position, requisite sulfinamide **9** could be prepared from aldehyde **8** using Ellman's *t*-butylsulfinimine methodology.[20] Protecting group manipulation was followed by conversion of bromide **9** to pinacolboronate **10**. Subsequent Suzuki coupling with the appropriate halide **14** was followed by deprotection to produce chiral biphenylamines **11a**−**g**. The biphenylamines could be processed as previously described for **7a**−**h** to afford final biphenylaminocyclopropane carboxamides **12a**−**g** and **13a**−**j**. The preparation of requisite halides **14a**−**e** is illustrated in Scheme 2.

Biological Results and Discussion. K_i values (nM) were determined radiometrically using the appropriate radioligand and Chinese hamster ovary (CHO) cells stably expressing the hB_1 or hB_2 receptor. In vitro functional activity was assessed in standard FLIPR experiments (IC_{50}, nM) employing functionally active hB_1 receptors. Studies of P-gp mediated directional transport were performed in LLC-PK1 cells expressing genes for human P-gp (MDR1), and the ratio of transport from basalateral to apical (B to A) direction to the ratio of transport from apical to basalateral (A to B) direction was measured. Full details for the previous experiments are described in the Experimental Procedures.

Table 1. Bradykinin B_1 Receptor Binding Affinities and P-gp Susceptibility

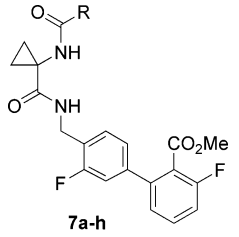

compound	R	hBK_1[a]	P-gp[b]	Papp[c]
2a	CH_2CF_3	0.81	18.4	23
7a	CF_2CF_3	2.95	2.2	31
7b	CF_3	1.47	4.1	23
7c	CHF_2	13.5	3.4	33
7d	CH_3	11.6	6.3	24
7e	$CHCl_2$	0.54	2.8	21
7f	CCH_3Cl_2	119	nd	nd
7g	$CClF_2$	2.5	2.8	29
7h	CHClF	2.8	nd	nd

[a] Values represent the numerical average of at least two experiments. Interassay variability was ±25% (K_i, nM). [b] MDR1 directional transport ratio (B/A)/(A/B). Values represent the average of three experiments, and interassay variability was ±20%. [c] Passive permeability (10^{-6} cm/s).

The trifluoropropionamide of lead structure **2** was replaced with various amides to identify compounds that would not be subject to human P-gp mediated efflux. After extensive screening, a series of polyhaloacetamides was found to be a promising lead. Data for key compounds **7a**−**h** are shown in Table 1. All compounds were B_1 selective (IC_{50} > 10 μM vs the B_2 receptor).

While replacement of the 3,3,3-trifluoroproprionamide in lead **2** with a pentafluoropropionamide led to about a 3-fold loss in

Table 2. Bradykinin B_1 Receptor Binding Affinities and Pgp Properties

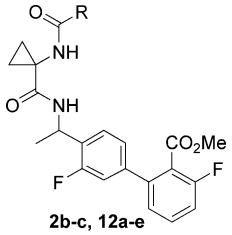

2b-c, 12a-e

compound	R	hBK_1[a]	P-gp[b]	Papp[c]
2b-(*R*)	CH_2CF_3	0.13	8.6	25
2c-(*S*)	CH_2CF_3	22	nd	nd
12a-(*R*)	CF_2CF_3	1.6	1.4	31
12b-(*R*)	CF_3	0.57	2.3	28
12c-(*R*)	CHF_2	0.4	3.2	31
12d-(*R*)	CH_3	0.93	8.6	21
12e-(*R*)	$CClF_2$	0.81	2.5	34

[a] Values represent the numerical average of at least two experiments. Interassay variability was ±25% (K_i, nM). [b] MDR1 directional transport ratio (B/A)/(A/B). Values represent the average of three experiments, and interassay variability was ±20%. [c] Passive permeability (10^{-6} cm/s).

hB_1 receptor binding affinity, it provided a major advance in that **7a** showed significantly reduced susceptibility to human P-gp medicated efflux (directional transport ratio of 2.2). Removal of the difluoromethylene from the amide in **2** provided trifluoroacetamide **7b**, which improved the binding potency but led to a slight increase in the P-gp susceptibility. Deletion of one or all of the fluorines (**7c**−**d**) gave a 10-fold loss in hB_1 receptor affinity without improvement in P-gp susceptibility. Dichloroacetamide **7e** provided the first subnanomolar compound (hK_i = 0.54 nM) with a promising P-gp directional transport ratio of 2.8. However, **7e** proved to be quite unstable and was eliminated from further consideration. Addition of a methyl group provided 2,2-dichloropropionamide **7f**, which had a deleterious effect on hB_1 binding. Mixed haloacetamides such as **7g**−**h** were similarly potent to **7a** with reasonable P-gp profiles.

An additional factor that warrants attention with relation to P-gp efflux is the passive permeability of a given compound, which can also influence CNS levels.[21] Compounds with low permeability tend to diminish the reliability that a P-gp transport assay can be used to predict CNS distribution. A passive permeability value of 15×10^{-6} cm/s or greater is typical for compounds that exhibit good levels of CNS penetration, and haloacetamides **7a**−**h** all met or exceeded this criterion.

The effects the polyhaloacetamides exert on P-gp transport are dramatic, but the underlying reason is less evident. One thought is that the increased lipophilicity due to the halogens reduces P-gp mediated transport. However, P-gp substrate **2a** is equal to or more lipophilic (log P 2.9) than several low transport compounds such as **7b** (log P 2.7), **7c** (log P 2.4), and **7e** (log P 2.8). In addition, the fewer hydrogen bond acceptors a compound possesses, the less likely it is to be a substrate for P-gp. Having the halogens alpha to the amide group is vital, indicating that a strong electronic withdrawing effect is active. We propose that the electron deficient amide is a poorer hydrogen bond acceptor and is therefore less prone to recognition by P-gp.[22]

The addition of a methyl group at the benzylic methylene has been shown to increase binding affinity in the aforesaid 2,3-diaminopyridine series.[16] Accordingly, compounds bearing this methyl group with select polyhaloacetamides from Table 1 were evaluated for their effects on hB_1 binding and on human P-gp transport (Table 2).

Addition of a methyl group proved to have favorable effects on both hB_1 receptor affinity and P-gp susceptibility. For example, the *R*-enantiomer **2b** was about 5-fold more potent (hK_i = 0.13 nM) than the des-methyl comparator **2a**, while *S*-**2c** gave a hK_i of 22 nM. Furthermore, the P-gp susceptibility was reduced 2-fold, establishing that the addition of a methyl group with the *R*-configuration not only increased potency but reduced the susceptibility to human P-gp mediated efflux. This proved general for polyhaloacetamides **12a**−**e** in Table 2. Among them, trifluoroacetamide **12b** represented a promising selection for further evaluation. Although **12b** was not significantly more potent than haloacetamides **12c**−**e,** nor did it possess the lowest P-gp transport ratio as compared to **12a**, it did embody the best combination of desirable properties required in a single compound.

Having focused in on trifluoroacetamide as the key discovery toward reducing the potential for P-gp mediated efflux, fine-tuning the pharmacokinetic (PK) properties became paramount. Drug metabolism studies have indicated that methyl ester hydrolysis was a major metabolic clearance pathway for compounds such as **12b**. A number of alterations to the C-ring ester and halogen substituents was made to scope their effects with respect to binding affinity, human P-gp efflux, and pharmacokinetic properties in the rat. Results are detailed in Table 3.

Removal of the fluorine atom ortho to the ester (**13a**) on the phenyl ring led to a to 20-fold loss in binding relative to **12b**, while having little impact on the P-gp profile. Replacement with the larger chlorine (**13b**), however, afforded an improvement in both P-gp efflux and Papp, while maintaining a very high B_1 receptor affinity with a hK_i of 0.44 nM. The size of the ester group is of consequence as the related ethyl ester **13c** was about 3-fold less potent than the methyl ester **13b**. Ester isosteres such as oxadiazoles **13d**−**e** maintained good receptor affinity but saw moderate increases in P-gp efflux. A similar observation was made with tetrazoles **13f**−**h**, particularly for the weakly active *N*-1 isomer **13h**. It is likely that the increases in P-gp efflux are a consequence of the enhanced hydrogen bond acceptor ability resulting from the additional nitrogen atoms in those heterocyclic rings. Other ester surrogates such as trifluoromethyl (**13i**) or an ethyl ketone (**13j**) conserved good P-gp and permeability profiles but are 2−3 times less active with respect to B_1 receptor binding affinity.

In terms of the pharmacokinetic profiles, going from trifluoropropionamide **2b** to trifluoroacetamide **12b** led to an increased clearance with a shorter half-life in the rat. Theaddition of the larger chlorine atom (**13b**) did increase bioavailability relative to **12b**, but no benefit in clearance or half-life was observed. As expected, the larger ethyl ester **13c**, which was assumed to be less prone to hydrolysis, had an improved rat profile as compared to the methyl ester. Surprisingly, the heterocyclic isosteres **13d**−**g** provided little benefit with regard to half-life as compared to their ester counterparts. Trifluoromethyl compound **13i** had a good rat PK with the best half-life in the series of 2.6 h. Taken as a whole, although a number of methyl ester replacements proved to sustain good B_1 receptor affinity, they offered no significant advantage in terms of PK and were more susceptible to P-gp mediated efflux. Consequently, the primary focus remained on the esters **12b** and **13b**.

The pharmacokinetic behavior of **12b** and **13b** was evaluated in the dog and monkey to further assess their potential for human PK projection. Although the oxadiazoles did not offer an advantage over the esters in terms of rat PK, oxadiazole **13d**

Table 3. Bradykinin B_1 Receptor Binding Affinities, P-gp Transport Properties, and Rat Pharmacokinetics

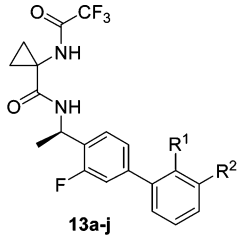

13a-j

Compound	R^1	R^2	hBK_1 [a] (nM)	h FLIPR (nM)	P-gp[b]	P_{app} (10^{-6} cm/s)[c]	Rat PK[d] F%, $t_{1/2}$, Cl
2b	CO_2Me	F	0.13	nd	8.6	25	14, 1.44, 25
12b	CO_2Me	F	0.57	1.9	2.3	20	21, 0.5, 42
13a	CO_2Me	H	10.3	nd	2.2	34	nd
13b	CO_2Me	Cl	0.44	1.52	1.9	34	34, 0.4, 40
13c	CO_2Et	Cl	1.35	9.1	2.1	25	45, 1.1, 8.4
13d		F	0.51	0.89	5.6	37	27, 0.35, 28
13e		F	0.68	nd	3.7	28	44, 0.34, 27
13f		F	0.6	0.65	4	33	48, 0.7, 11
13g		Cl	0.66	nd	5.5	29	50, 0.7, 12
13h		F	62.5	nd	15.5	19	nd
13i	CF_3	F	1.44	7.3	2	32	30, 2.6, 10
13j	COEt	Cl	1.95	nd	1.6	27	nd

[a] Values represent the numerical average of at least two experiments. Interassay variability was ±25% (K_i, nM) and ±25% for the FLIPR experiments (IC_{50}, nM). [b] MDR1 directional transport ratio (B/A)/(A/B). Values represent the average of three experiments and interassay variability was ±20%. [c] Passive permeability (10^{-6} cm/s). [d] F% oral bioavailability, half-life is represented in hours, Cl in mL/min/kg. Sprague−Dawley rats ($n = 3$). Oral dose = 10 mg/kg, IV dose = 2 mg/kg. Interanimal variability was less than 20%.

Table 4. Rat and Dog Pharmacokinetics for Select Compounds

	dog PK[a]			Rhesus PK[b]		
compound	*F* (%)	$t_{1/2}$ (h)	Cl mL/min/kg	*F* (%)	$t_{1/2}$ (h)	Cl mL/min/kg
12b	5	1.7	21	2	2.2	28
13b	33	1.8	9	31	1.7	13
13d	35	3.9	6	22	2.9	15

[a] Mongrel dogs ($n = 2$). Oral dose 3 mg/kg and IV dose = 1 mg/kg. Interanimal variability was less than 20% for all values. [b] Rhesus monkies ($n = 2$). Oral dose 3 mg/kg and IV dose = 1 mg/kg. Interanimal variability was less than 20% for all values.

was included to see if this ester surrogate offered improvement in these species. Results are shown in Table 4.

Methyl ester **12b** had extremely poor bioavailability (<5%) and rapid clearance in both dog and rhesus. Replacement of the fluorine with a chlorine ortho to the methyl ester (**13b**) significantly improved the oral bioavailability and reduced the clearance to an acceptable level in both species. Incorporation of the oxadiazole (**13d**) showed good bioavailability and improved the half-lives in dog and rhesus relative to the methyl esters. However, since **13d** was subject to human P-gp mediated efflux (P-gp = 5.6), it was eliminated from further consideration. Although compounds **12b** and **13b** exhibited only fair pharmacokinetic properties, they demonstrated superior stability in human microsomes and hepatocytes (see Supporting Information) relative to the three species, indicating that they were likely to have adequate bioavailability in humans.

Pharmacodynamic Models. Previously, the 2,3-diaminopyridine series of bradykinin B_1 antagonists proved to be selective for the human and rabbit over the rat receptor, thwarting efforts to characterize lead compounds in classic rodent models of pain and inflammation.[15] Similarly, the biphenylaminocyclopropane carboxamide series described here has shown a similar selectivity but also exhibits a high affinity for the rhesus bradykinin B_1 receptor as exemplified by **13b** in Table 5.

Accordingly, as one pharmacodynamic model, we induced functional receptors in the rhesus vasculature by iv administration of lipopolysaccharide (LPS), an effect that is manifest by a depressor blood pressure response to the B_1 agonist DAK (1

Table 5. Species Differences and In Vivo Experiments for Compound **13b**

human K_i (nM)[a]	0.4
rat K_i (nM)[a]	1646
rabbit K_i (nM)[a]	7.3
Rhesus K_i (nM)[a]	2.0
Rhesus LPS AD_{90} (μg/Kg)[b]	47 ± 10
transgenic rat Occ_{90} (nM)[b]	520

[a] Values represent the numerical average of at least two experiments. Interassay variability was ±25% for the binding assays (K_i, nM). [b] IV dosing, see Experimental Procedures for full assay details.

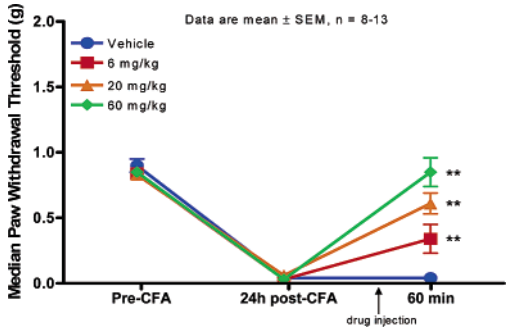

Figure 2. Reversal of CFA-induced hypersensitivity by **13b** in hB_1 knock-in mice.

μg kg iv).[23] Generation of antagonist dose−responses to the depressor effects were created by pretreatment with rising doses of **13b** prior to treatment with DAK. In this model, **13b** proved highly potent to block the depressor effect with an AD_{90} of 47 μg/kg.

To measure the facility with which **13b** binds to the human B_1 receptor expressed in the CNS, we employed the previously described transgenic rat model.[24] While the human B_1 receptors expressed in this particular transgenic rat model do not appear to be functional, this model does serve as a useful tool to demonstrate CNS receptor occupancy using an ex vivo binding assay. Since there is currently no animal pain model with which one can correlate CNS occupancy with efficacy, our goal was to achieve high (i.e., 90%) brain receptor occupancy (Occ_{90}) in the transgenic rat. Compound **13b** exhibited an Occ_{90} of 520 nM in the rat CNS, a reasonable brain level that should be attainable in humans based on its low substrate activity at P-gp.

Recently, a human selective B_1 antagonist has been shown to be efficacious in reducing complete Freund's adjuvant (CFA)-induced mechanical hyperalgesia in humanized but not wild-type mice.[25] Accordingly, we decided to evaluate antagonist **13b** in a CFA-induced hyperalgesia model employing a similar human B_1 knock-in mouse. This particular mouse model utilized gene targeting by homologous recombination to replace the genomic sequence for the endogenous mouse B_1 receptor with that of the human B_1 receptor.[26] This B_1 knock-in mouse has been shown to possess the pharmacological characteristics consistent with the human B_1 receptor being expressed and regulated physiologically.

As expected, injection of CFA into the left hind paw of the human B_1 knock-in mice produced inflammation and a decrease in tactile withdrawal threshold (hyperalgesia) in the affected hind paw when measured 24 h following CFA injection (Figure 2). The paw withdrawal thresholds of CFA injected mice were unaffected by vehicle treatment. Compound **13b** was dosed orally at 6, 20, and 60 mg/kg, which resulted in plasma concentrations of 1.0, 3.5, and 5.0 μM, respectively, at 1 h. Oral administration of compound **13b** dose dependently reversed the hyperalgesia in hB_1 knock-in mice with an ED_{50} (95% CL) = 9.76 (6.0−15.8) mg/kg (Figures 2 and 3). Moreover, the

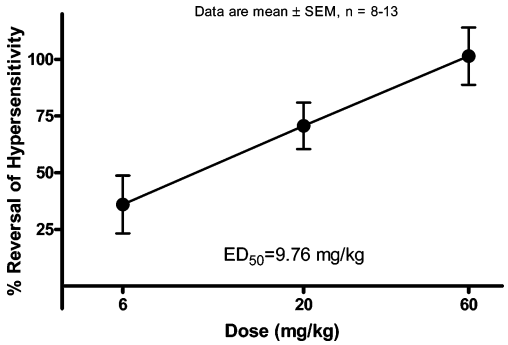

Figure 3. Dose−response curve of **13b** (p.o.) in hB_1 knock-in mice.

efficacy produced by the maximum dose of 60 mg/kg (100%) was similar to that observed with the NSAID naproxen in this model (50%, data not shown). It should be noted that CFA injection produced equivalent hyperalgesia in the wild-type mice, which was unaffected by oral administration of **13b** (Supporting Information).

While **13b** was not subject to human P-gp efflux (transport ratio of 1.9), it was a substrate for mouse P-gp efflux in vitro in LLC-PK1 cells (transport ratio of 9.3). To correlate how the observed human P-gp transport ratios may affect CNS levels, we investigated in vivo studies in P-gp deficient and competent mice. P-gp had little impact on the plasma clearance of **13b** indicated by the AUCs [p(−)/p(++) = 1.2], but a 9-fold reduction in brain exposure was observed for P-gp competent mice [AUCs b(−)/b(++) = 9.1]. The ratio of brain to plasma [b(−)/p(−)]for **13b** in P-gp deficient mice is 1.05, demonstrating excellent brain penetration in the absence of P-gp. We believe that this will be similar to the case in man since **13b** is not a human P-gp substrate and should exhibit good brain penetration. To validate this result with a primate model, CNS levels in a Rhesus monkey were taken (2 mpk iv, 30 min) and found to give an adequate brain/plasma ratio of 0.4.

Conclusion

We have identified trifluoromethyl carboxamide **13b** as a potent antagonist for the human bradykinin B_1 receptor that demonstrated significantly reduced susceptibility to human P-gp mediated efflux. The compound shows good potential for human CNS penetration based on brain levels in CF-1 mice and monkeys. Additionally, **13b** also exhibited good CNS receptor occupancy in the transgenic rat expressing the human B_1 receptor and showed oral efficacy in reducing CFA-induced hyperalgesia in a humanized mouse. On the basis of these properties and the potential for good human pharmacokinetics, compound **13b** was selected as a development candidate for the treatment of pain and inflammation.

Experimental Procedures

General. All commercially available chemicals and solvents were used without further purification. ^{1}H (400 MHz) NMR spectra were recorded on a Varian VXR 400 spectrometer unless otherwise noted. The chemical shifts are reported in δ (ppm) using the δ 0.00 signal of Me_4Si as an internal standard. High resolution MS data were obtained on a Bruker Daltonics FTICR/MS. High resolution mass spectral analysis was performed on a Bruker-daltonics BioApex 3T mass spectrometer. All animal studies described herein were approved by the Merck Research Laboratories Institutional Animal Care and Use Committee. HPLC spectra were recorded on a Hewlett-Packard 1100 with a CombiScreen Pro C18 column. The purity of compounds was assessed to be >95% by analytical HPLC: (i) system 1: linear gradient over 10 min of CH_3CN/0.1% TFA and H_2O/0.1% TFA 10:90 to 95:5 and 2 min at 95:5; flow

rate 1.0 mL/min; detection at 215 and 254 nm (YMC-Pack Pro C18, 50 mm × 4.6 mm column). (ii) Linear gradient over 3.5 min of CH_3CN/0.1% TFA and H_2O/0.1% TFA 5:95 to 95:5; flow rate 1.5 mL/min; detection at 215 nm (YMC-Pack Pro C18, 50 mm × 4.6 mm column).

Methyl 4′-(Aminomethyl)-3,3′-difluoro-1,1′-biphenyl-2-carboxylate (5). To a heat-dried flask under N_2 was added methyl 2-fluoro-6-iodobenzoate (5.00 g, 17.9 mmol) and Rieke Zn (Aldrich, 5 g in 100 mL of THF, 0.765 M THF, 24.5 mL, 18.8 mmol). The reaction was heated to 90 °C for 4.5 h. To the crude zinc iodide was added a solution of 4-bromo-2-fluorobenzonitrile (3.57 g, 17.9 mmol) in THF (5 mL) and $Pd(PPh_3)_4$ (0.100 g, 0.086 mmol). The mixture was heated to reflux for 1 h, cooled to room temperature, and concentrated in vacuo. The resultant residue was dissolved in EtOAc and filtered through celite. The filtrate was washed with H_2O and brine, dried over Na_2SO_4, filtered, and concentrated. The residue was subjected to silica gel chromatography (0−10% EtOAc in hexanes) to provide methyl 4′-cyano-3,3′-difluoro-1,1′-biphenyl-2-carboxylate as an orange solid.

To a solution of the methyl 4′-cyano-3,3′-difluoro-1,1′-biphenyl-2-carboxylate (1.30 g, 4.76 mmol) in NH_3 in MeOH (2.0 M, 20 mL, 40 mmol) was added Raney Nickel (suspension in H_2O, ∼0.25 g). The solution was placed under an atmosphere of H_2 (balloon) and stirred at room temperature overnight. The mixture was filtered through glass filter paper and concentrated in vacuo. The residue was azeotroped 3 times with toluene and partitioned between 1 N HCl and EtOAc. The organic layer was washed 2 times with 1 N HCl. Aqueous NaOH (1 M) was added to pH ∼10, and the product was extracted 3 times with EtOAc. The combined organic fractions were dried over Na_2SO_4, filtered, and concentrated to provide **5** (0.89 g, 68%). ^{1}H NMR (400 MHz, $CDCl_3$) δ 1.53 (s, 2H), 3.74 (s, 3H), 3.95 (s, 2H), 7.05−7.18 (m, 4H), 7.35−7.49 (m, 2H).

1-[({[3,3′-Difluoro-2′-(methoxycarbonyl)-1,1′-biphenyl-4-yl]-methyl}amino)carbonyl]cyclopropanaminium Chloride (6). Compound **5** (0.620 g, 2.24 mmol) was dissolved in EtOAc (10 mL), cooled to 0 °C, and saturated with HCl (g). After 30 min at room temperature, the mixture was concentrated in vacuo. A solution of this crude salt, (∼0.70 g, 2.2 mmol), *tert*-butoxycarbonyl-1-aminocyclopropane-1-carboxylic acid (0.494 g, 2.45 mmol), 1-ethyl-(3-dimethylaminopropyl)carbodiimide hydrochloride (0.855 g, 4.46 mmol), 1-hydroxy-7-azabenzotriazole (0.010 g, 0.15 mmol), and triethylamine (1.35 g, 13.4 mmol) in CH_2Cl_2 (15 mL) was stirred at room temperature overnight. The solution was washed with aqueous sodium bicarbonate and brine, dried over Na_2SO_4, filtered, and concentrated. The residue was subjected to silica gel chromatography (10−50% EtOAc in hexanes) to provide methyl 4′-{[({1-[(*tert*-butoxycarbonyl)amino]cyclopropyl}carbonyl)amino]methyl}-3,3′-difluoro-1,1′-biphenyl-2-carboxylate (1.04 g, 100%) as a white solid. This Boc protected amine was dissolved in EtOAc (10 mL), cooled to 0 °C, and saturated with HCl (g). After 30 min at room temperature, the mixture was concentrated in vacuo. The residue was azeotroped 3 times with toluene to provide the hydrochloride salt of **6** as a white solid. ^{1}H NMR (400 MHz, CD_3OD) δ 1.37−1.40 (m, 2H), 1.53−1.57 (m, 2H), 3.68 (s, 3H), 4.47 (s, 2H), 7.07−7.14 (m, 2H), 7.21−7.25 (m, 2H), 7.37 (t, J = 7.7 Hz, 1H), 7.52−7.57 (m, 1H). MS m/z = 361.22 (MH^+).

General Procedure for the Preparation of Compounds 7a−h. Methyl 3,3′-Difluoro-4′-{[({1-[(2,2,3,3,3-pentafluoropropanoyl)-amino]cyclopropyl}carbonyl)amino]methyl}-1,1′-biphenyl-2-carboxylate (7a). A solution of **6** (48.4 mg, 0.12 mmol), pentafluoropropionic acid (40.0 mg, 0.24 mmol), 1-ethyl-(3-dimethylaminopropyl)carbodiimide hydrochloride (46.8 mg, 0.24 mmol), 1-hydroxy-7-azabenzotriazole (0.010 g, 0.15 mmol), and triethylamine (74.1 mg, 0.73 mmol) in DMF (2 mL) was stirred at room temperature overnight. The mixture was diluted with EtOAc, washed with aqueous sodium bicarbonate and brine, dried over Na_2SO_4, filtered, and concentrated. The residue was purified via reversed phase HPLC to provide **7a** (10 mg, 16%) as a white solid. ^{1}H NMR (400 MHz, CD_3OD) δ 1.06−1.09 (m, 2H), 1.55−1.58 (m, 2H), 3.68 (s, 1H), 7.20−7.26 (m, 2H), 7.07−7.13 (m, 2H), 7.38 (t, J = 8.0 Hz, 1H), 7.55 (q, J = 8.0 Hz, 1H), 8.53 (s, 1H), 9.95 (s, 1H). MS m/z = 507.25 (MH^+). Anal. ($C_{22}H_{17}F_7N_2O_4$•H_2O) C, H, N.

Methyl 3,3′-Difluoro-4′-{[({1-[(trifluoroacetyl)amino]cyclopropyl}carbonyl)amino]methyl}-1,1′-biphenyl-2-carboxylate (7b). White solid: yield 66%. ^{1}H NMR (400 MHz, CD_3OD) δ 1.12 (q, J = 4.2 Hz, 2H), 1.55 (q, J = 4.2 Hz, 2H), 2.68 (s, 3H), 4.49 (s, 2H), 7.05−7.14 (m, 2H), 7.22−7.28 (m, 2H), 7.40 (t, J = 7.8 Hz, 1H), 7.54−7.61 (m, 1H). HRMS Calcd for $C_{21}H_{18}F_5N_2O_4$ (M+1): 457.1186. Found: 457.1182. Anal. ($C_{21}H_{17}F_5N_2O_4$) C, H, N.

Methyl 4′-{[({1-[(Difluoroacetyl)amino]cyclopropyl}carbonyl)-amino]methyl}-3,3′-difluoro-1,1′-biphenyl-2-carboxylate (7c). White solid: yield 34%. ^{1}H NMR (400 MHz, CD_3OD) δ 1.10 (q, J = 4.5 Hz, 2H), 1.53 (q, J = 4.5 Hz, 2H), 3.68 (s, 3H), 4.49 (s, 2H), 6.03 (t, J = 54.0 Hz, 1H), 7.05−7.14 (m, 2H), 7.19−7.25 (m, 2H), 7.39 (t, J = 7.8 Hz, 1H), 7.51−7.58 (m, 1H). HRMS Calcd for $C_{21}H_{19}F_4N_2O_4$ (M+1): 439.1281. Found: 439.1271. Anal. ($C_{21}H_{18}F_4N_2O_4$•0.85 CH_2Cl_2) C, H, N.

Methyl 4′-[({[1-(Acetylamino)cyclopropyl]carbonyl}amino)-methyl]-3,3′-difluoro-1,1′-biphenyl-2-carboxylate (7d). White solid: yield 54%. ^{1}H NMR (400 MHz, CD_3OD) δ 1.04 (q, J = 4.5 Hz, 2H)c 4.49 (q, J = 4.5 Hz, 2H), 3.70 (s, 3H), 4.51 (d, J = 5.9 Hz, 2H), 7.06−7.15 (m, 2H), 7.21−7.27 (m, 2H), 7.42 (t, J = 7.9 Hz, 1H), 7.52−7.60 (m, 1H), 8.52 (t, J = 5.9 Hz, 1H). HRMS Calcd for $C_{21}H_{21}F_2N_2O_4$ (M + 1): 403.1469. Found: 403.1459. Anal. ($C_{21}H_{20}F_2N_2O_4$•0.35 CH_2Cl_2) C, H, N.

Methyl 4′-{[({1-[(Dichloroacetyl)amino]cyclopropyl}carbonyl)-amino]methyl}-3,3′-difluoro-1,1′-biphenyl-2-carboxylate (7e). White solid: yield 71%. ^{1}H NMR (400 MHz, CD_3OD) δ 1.08 (q, J = 4.6 Hz, 2H), 1.54 (q, J = 4.6 Hz, 2H), 3.68 (s, 3H), 4.50 (s, 2H), 6.24 (s, 1H), 7.05−7.14 (m, 2H), 7.19−7.25 (m, 2H), 7.39 (t, J = 7.8 Hz, 1H), 7.51−7.58 (m, 1H). HRMS Calcd for $C_{21}H_{19}Cl_2F_2N_2O_4$ (M + 1): 471.0690. Found: 471.0681. Anal. ($C_{21}H_{18}Cl_2F_2N_2O_4$•0.4 H_2O) C, H, N.

Methyl 4′-{[({1-[(2,2-Dichloropropanoyl)amino]cyclopropyl}-carbonyl)amino]methyl}-3,3′-difluoro-1,1′-biphenyl-2-carboxylate (7f). White solid: yield 23%. ^{1}H NMR (400 MHz, CD_3OD) δ 1.11 (q, J = 4.8 Hz, 2H), 1.54 (q, J = 4.8 Hz, 2H), 2.28 (s, 3H), 3.68 (s, 3H), 4.51 (s, 2H), 7.06−7.14 (m, 2H), 7.20−7.26 (m, 2H), 7.40 (t, J = 7.8 Hz, 1H), 7.51−7.58 (m, 1H). HRMS Calcd for $C_{22}H_{21}Cl_2F_2N_2O_4$ (M+1): 485.0846. Found: 485.0835.

Methyl 4′-({[(1-{[Chloro(difluoro)acetyl]amino}cyclopropyl)-carbonyl]amino}methyl)-3,3′-difluoro-1,1′-biphenyl-2-carboxylate (7g). White solid: yield 34%. ^{1}H NMR (400 MHz, CD_3OD) δ 1.11 (q, J = 4.6 Hz, 2H), 1.55 (q, J = 4.6 Hz, 2H), 3.68 (s, 3H), 4.49 (s, 2H), 7.05−7.14 (m, 2H), 7.19−7.26 (m, 2H), 7.38 (t, J = 7.8 Hz, 1H), 7.51−7.58 (m, 1H). HRMS Calcd for $C_{21}H_{18}ClF_4N_2O_4$ (M + 1): 473.0891. Found: 473.0880. Anal. ($C_{21}H_{17}ClF_4N_2O_4$•0.5H_2O) C, H, N.

Methyl 4′-({[(1-{[Chloro(fluoro)acetyl]amino}cyclopropyl)-carbonyl]amino}methyl)-3,3′-difluoro-1,1′-biphenyl-2-carboxylate (7h). White solid: yield 32%. ^{1}H NMR (400 MHz, CD_3OD) δ 1.04−1.15 (m, 2H), 1.58−1.69 (m, 2H), 3.73 (s, 3H), 4.51 (d, J = 6.1 Hz, 2H), 6.29 (d, J = 50.5 Hz, 1H), 6.78 (t, J = 6.0 Hz, 1H), 7.02−7.16 (m, 4H), 7.27−7.49 (m, 3H). MS m/z = 455.11 (MH^+). Anal. ($C_{21}H_{18}ClF_3N_2O_4$) C, H, N.

***N*-[(1*R*)-1-(4-Bromo-2-fluorophenyl)ethyl]-2-methylpropane-2-sulfinamide (9).** To a solution of (*S*)-(−)-2-methyl-2-propanesulfinamide (20.20 g, 0.167 mol) in 350 mL of CH_2Cl_2 was added 4-bromo-2-fluorobenzaldehyde (35.53 g, 0.1750 mol), pyridinium *p*-toluenesulfonate (2.09 g, 8.33 mmol), and magnesium sulfate (200.6 g, 1.667 mol). The reaction was stirred at room temperature for 48 h. More magnesium sulfate (100.3 g, 0.833 mol) was added, and the reaction was stirred for an additional 24 h. The mixture was filtered through celite, washed with CH_2Cl_2, and concentrated in vacuo. The resulting residue was subjected to silica gel chromatography (0−10% ethyl acetate in hexanes) to provide *N*-[(1*E*)-(4-bromo-2-fluorophenyl)methylidene]-2-methylpropane-2-sulfinamide (24.83 g, 48%) as a white solid: ^{1}H NMR (400 MHz, $CDCl_3$) δ 1.27 (s, 9H), 7.35−7.41 (m, 2H), 7.87 (t, J = 7.8 Hz, 1H), 8.83 (s, 1H). MS m/z 308 (MH^+).

To a solution of the aforementioned imine (32.6 g, 0.106 mol) in CH_2Cl_2 (550 mL) at −48 °C was added methylmagnesium chloride (3.0 M solution in ether, 53.3 mL, 0.160 mol) dropwise over 1 h. The reaction was quenched with aqueous ammonium chloride, and the aqueous layer was extracted with CH_2Cl_2. The combined organics were dried over Na_2SO_4, filtered, and concentrated in vacuo. The resulting residue was subjected to silica gel chromatography (10−50% EtOAc in hexanes) to provide **9** (22.6 g, 65%) as a white solid: ^{1}H NMR (400 MHz, $CDCl_3$) δ 1.19 (s, 9H), 1.56 (d, J = 6.8 Hz, 3H), 3.33 (d, J = 4.2 Hz, 1H), 4.77−4.85 (m, 1H), 7.21−7.29 (m, 3H). MS m/z 324.11 (MH^+).

***tert*-Butyl (1*R*)-1-[2-Fluoro-4-(4,4,5,5-tetramethyl-1,3,2-dioxaborolan-2-yl)phenyl]ethylcarbonate (10).** To a solution of **9** (26.29 g, 81.58 mmol) in MeOH (40 mL) was added HCl in a dioxane (4 M, 40.8 mL, 0.163 mol) solution. The reaction mixture was concentrated in vacuo, and ether was added. The white solid was collected, washed with cold ether, and dried in vacuo to provide (1*R*)-1-(4-bromo-2-fluorophenyl)ethanaminium chloride (14.2 g, 98%) as a white solid: ^{1}H NMR (400 MHz, CD_3OD) δ 1.64 (d, J = 6.8 Hz, 3H), 4.70 (q, J = 6.8 Hz, 1H), 7.41−7.52 (m, 3H). MS m/z 203.14 (MH^+).

To a solution of (1*R*)-1-(4-bromo-2-fluorophenyl)ethanaminium chloride (14.3 g, 55.9 mmol) in CH_2Cl_2 (300 mL) at 0 °C was added di(*tert*-butyl) dicarbonate (17.98 g, 82.40 mmol) and triethylamine (8.25 g, 81.6 mmol). The solution was washed with water and brine, dried over Na_2SO_4, filtered, and concentrated in vacuo to provide crude *tert*-butyl (1*R*)-1-(4-bromo-2-fluorophenyl)-ethylcarbamate (30.2 g, 100%) as a white solid: ^{1}H NMR (400 MHz, $CDCl_3$) δ 1.41 (br s, 9H), 1.53 (s, 3H), 4.91 (s, 1H), 7.13−7.24 (m, 3H).

A mixture of *tert*-butyl (1*R*)-1-(4-bromo-2-fluorophenyl)ethylcarbamate (26.4 g, 83.1 mmol), bis(pinacolato)diboron (31.6 g, 0.125 mol), potassium acetate (24.5 g, 0.249 mol), and [1,1′-bis-(diphenylphosphino)ferrocene]palladium(II) dichloride (0.26 g, 0.36 mmol) in DMSO (80 mL) was heated to 90 °C under N_2 for 3 h. The mixture was then cooled to room temperature and partitioned between EtOAc and water. The organic extract was washed with water and brine, dried over Na_2SO_4, filtered, and concentrated in vacuo. The residue was subjected to silica gel chromatography (0−10% EtOAc in hexanes) to provide **10** (32.0 g, 100%) as a beige solid: ^{1}H NMR (400 MHz, $CDCl_3$) δ 1.26 (s, 12H), 1.33 (s, 9H), 1.52 (s, 3H), 4.97 (s, 1H), 7.27−7.29 (m, 1H), 7.44 (d, J = 11.2 Hz, 1H), 7.53 (d, J = 7.5 Hz, 1H).

General Procedure for the Preparation of Compounds 11a−g. Methyl 4′-{(1*R*)-1-[(*tert*-Butoxycarbonyl)amino]ethyl}-3-chloro-3′-fluoro-1,1′-biphenyl-2-carboxylate (11b). A mixture of methyl 2-bromo-6-chlorobenzoate (2.25 g, 9.03 mmol), *tert*-butyl (1*R*)-1-[2-fluoro-4-(4,4,5,5-tetramethyl-1,3,2-dioxaborolan-2-yl)phenyl]ethylcarbonate **10** (3.00 g, 8.21 mmol), potassium carbonate (2.84 g, 20.5 mmol), tri-*o*-tolylphosphine (0.10 g, 0.33 mmol), and palladium acetate (0.018 g, 0.08 mmol) in THF (40 mL) and water (4 mL) was heated in a sealed flask at 100 °C for 4 h. The mixture was then cooled and concentrated in vacuo. The resulting residue was dissolved in EtOAc, washed with water and brine, dried over Na_2SO_4, filtered, and concentrated in vacuo to provide methyl 4′-{(1*R*)-1-[(*tert*-butoxycarbonyl)amino]ethyl}-3-chloro-3′-fluoro-1,1′-biphenyl-2-carboxylate as a white solid.

The Boc protected amine was dissolved in EtOAc (20 mL), cooled to 0 °C, and saturated with HCl (g). After 30 min at room temperature, the mixture was concentrated in vacuo. The residue was azeotroped 3 times with toluene to provide (1*R*)-1-[3′-chloro-3-fluoro-2′-(methoxycarbonyl)-1,1′-biphenyl-4-yl]ethanaminium chloride. The product was partitioned between EtOAc and aqueous sodium bicarbonate. The organic layer was washed with brine, dried over Na_2SO_4, filtered, and concentrated in vacuo to provide **11b** (1.79 g, 70%) as a yellow oil: ^{1}H NMR (400 MHz, $CDCl_3$) δ 1.44 (d, J = 6.6 Hz, 3H), 1.58 (s, 2H), 3.74 (s, 3H), 4.41 (q, J = 6.6 Hz, 1H), 7.04−7.16 (m, 2H), 7.27−7.30 (m, 1H), 7.37−7.47 (m, 3H). The crude compounds were then taken directly onto **12a−e** and **13a−j**.

General Procedure for the Preparation of Compounds 12a−e and 13a−j. Methyl 3-Chloro-3′-fluoro-4′-{(1*R*)-1-[({1-[(trifluoroac-etyl)amino]cyclopropyl}carbonyl)amino]ethyl}-1,1′-biphenyl-2-carboxylate (13b). A solution of the HCl salt of **11b** (1.00 g, 2.91 mmol), *tert*-butoxycarbonyl-1-aminocyclopropane-1-carboxylic acid (0.614 g, 3.05 mmol), 1-ethyl-(3-dimethylaminopropyl)carbodiimide hydrochloride (1.11 g, 5.81 mmol), 1-hydroxy-7-azabenzotriazole (0.010 g, 0.15 mmol), and triethylamine (1.76 g, 17.4 mmol) in CH_2Cl_2 (20 mL) was stirred at room temperatue overnight. The solution was washed with aqueous sodium bicarbonate and brine, dried over Na_2SO_4, filtered, and concentrated in vacuo. The residue was subjected to silica gel chromatography (10−40% EtOAc in hexanes) to provide methyl 4′-{(1*R*)-1-[({1-[*tert*-butoxycarbonyl)amino]cyclopropyl}carbonyl)amino]ethyl}-3-chloro-3′-fluoro-1,1′-biphenyl-2-carboxylate (1.38 g, 96%) as a white solid: ^{1}H NMR (400 MHz, $CDCl_3$) δ 0.98−1.06 (m, 2H), 1.46 (s, 9H), 1.51−1.61 (m, 5H), 3.73 (s, 3H), 5.07 (br s, 1H), 5.22−5.32 (m, 1H), 7.00 (br s, 1H), 7.05−7.13 (m, 2H), 7.23−7.26 (m, 1H), 7.29−7.37 (m, 1H), 7.40−7.45 (m, 2H). MS m/z 491.30 (MH^+).

The product was dissolved in EtOAc (10 mL) and cooled to 0 °C, and the solution was saturated with HCl (g). After 30 min at room temperature, the mixture was concentrated in vacuo. The residue was azeotroped 3 times with toluene to provide 1-[({(1*R*)-1-[3′-chloro-3-fluoro-2′-(methoxycarbonyl)-1,1′-biphenyl-4-yl]ethyl}-amino)carbonyl]cyclopropanaminium chloride as a white solid: MS m/z 391.21 (MH^+).

To a solution of the previous product (13.60 g, 31.83 mmol) in CH_2Cl_2 (150 mL) and triethylamine (6.44 g, 6.36 mmol) at 0 °C was added trifluoroacetic anhydride (6.68 g, 3.18 mmol). The solution was diluted with additional CH_2Cl_2 and washed with aqueous sodium bicarbonate and brine, dried over Na_2SO_4, filtered, and concentrated. The residue was subjected to silica gel chromatography (10−40% EtOAc in hexanes) to provide **13b** (13.5 g, 87.1%) as a white solid: ^{1}H NMR (400 MHz, CD_3OD) δ 1.03−1.27 (m, 2H), 1.49−1.52 (m, 5H), 3.69 (s, 3H), 5.31 (q, J = 7.1 Hz, 1H), 7.07−7.17 (m, 2H), 7.33−7.51 (m, 4H). MS m/z = 487.22 (MH^+). Anal. ($C_{22}H_{19}ClF_4N_2O_4$) C, H, N.

Methyl 3,3′-Difluoro-4′-{(1*R*)-1-[({1-[(2,2,3,3-tetrafluoropropanoyl)amino]cyclopropyl}carbonyl)amino]ethyl}-1,1′-biphenyl-2-carboxylate (12a). White solid: yield 7%. ^{1}H NMR (400 MHz, CD_3OD) δ 1.01−1.15 (m, 2H), 1.41−1.55 (m, 5H), 3.68 (s, 3H), 5.22−5.32 (m, 1H), 6.38 (tt, J = 5.1, 52.5 Hz, 1H), 7.06−7.14 (m, 2H), 7.20−7.26 (m, 2H), 7.39 (t, J = 7.9 Hz, 1H), 7.51−7.58 (m, 1H), 7.77(d, J = 7.6 Hz, 1H), 9.73 (s, 1H). MS m/z = 503.26 (MH^+). Anal. ($C_{23}H_{20}F_6N_2O_4$.0.45 CH_2Cl_2) C, H, N.

Methyl 3,3′-Difluoro-4′-{(1*R*)-1-[({1-[(trifluoroacetyl)amino]-cyclopropyl}carbonyl)amino]ethyl}-1,1′-biphenyl-2-carboxylate (12b). White solid: 95.1%. ^{1}H NMR (400 MHz, CD_3OD) δ 1.02−1.16 (m, 2H), 1.49−1.51 (m, 5H), 3.68 (s, 3H), 4.86 (s, 2H), 5.30 (q, J = 7.1 Hz, 1H), 7.05−7.14 (m, 2H), 7.19−7.26 (m, 2H), 7.41 (t, J = 7.9 Hz, 1H), 7.51−7.58 (m, 1H). MS m/z = 471.23 (MH^+). Anal. ($C_{22}H_{19}F_5N_2O_4$.0.5 H_2O) C, H, N.

Methyl 4′-{(1*R*)-1-[({1-[(Difluoroacetyl)amino]cyclopropyl}-carbonyl)amino]ethyl}-3,3′-difluoro-1,1′-biphenyl-2-carboxylate (12c). White solid: 51%. ^{1}H NMR (400 MHz, CD_3OD) δ 1.01−1.15 (m, 2H), 1.45−1.52 (m, 5H), 3.69 (s, 3H), 5.30−5.34 (m, 1H), 6.08 (t, J = 54.0 Hz, 1H), 7.06−7.15 (m, 2H), 7.20−7.26 (m, 2H), 7.43 (t, J = 7.9 Hz, 1H), 7.52−7.59 (m, 1H), 8.21 (d, J = 7.6 Hz, 1H). MS m/z = 453.19 (M + H^+). Anal. ($C_{22}H_{20}F_4N_2O_4$.0.2 H_2O) C, H, N.

Methyl 4′-[(1*R*)-1-({[1-(Acetylamino)cyclopropyl]carbonyl}-amino)ethyl]-3,3′-difluoro-1,1′-biphenyl-2-carboxylate (12d). White solid: 36%. ^{1}H NMR (400 MHz, CD_3OD) δ 0.98−1.06 (m, 2H), 1.39−1.49 (m, 2H), 1.50 (d, J = 7.1 Hz, 3H), 2.02 (s, 3H), 3.69 (s, 3H), 5.27−5.35 (m, 1H), 7.05−7.15 (m, 2H), 7.20−7.26 (m, 2H), 7.45 (t, J = 8.1 Hz, 1H), 7.52−7.59 (m, 1H), 8.10 (d, J = 8.1 Hz, 1H). MS m/z = 417.23 (MH^+). Anal. ($C_{22}H_{22}F_2N_2O_4$.0.7 H_2O) C, H, N.

Methyl 4′-((1*R*)-1-{[(1-{[Chloro(difluoro)acetyl]amino}cyclopropyl)carbonyl]amino}ethyl)-3,3′-difluoro-1,1′-biphenyl-2-carboxylate (12e). White solid: yield: 70%. ^{1}H NMR (400 MHz,

CD_3OD) δ 1.02−1.16 (m, 2H), 1.46−1.55 (m, 5H), 3.68 (s, 3H), 5.29 (q, J = 7.1 Hz, 1H), 7.05−7.24 (m, 2H), 7.20−7.26 (m, 2H), 7.41 (t, J = 7.9 Hz, 1H), 7.51−7.58 (m, 1H). MS m/z = 487.14 (MH^+). Anal. ($C_{22}H_{19}ClF_4N_2O_4$•0.3 H_2O) C, H, N.

Methyl 3′-Fluoro-4′-{(1*R*)-1-[({1-[(trifluoroacetyl)amino]-cyclopropyl}carbonyl)amino]ethyl}-1,1′-biphenyl-2-carboxylate (13a). White solid: yield 22%. ^{1}H NMR (400 MHz, CD_3OD) δ 1.02−1.16 (m, 2H), 1.47−1.56 (m, 5H), 3.64 (s, 3H), 5.32 (q, J = 7.1 Hz, 1H), 6.97−7.06 (m, 2H), 7.35−7.40 (m, 2H), 7.46 (dot, J = 1.2, 7.6 Hz, 1H), 7.58 (dot, J = 1.5, 7.6 Hz, 1H), 7.78 (dd, J = 1.3, 7.6 Hz, 1H). HRMS Calcd for $C_{22}H_{24}F_4N_3O_4$ (M+NH^+): 470.1703. Found: 470.1694. Anal. ($C_{22}H_{20}F_4N_2O_4$•0.5 H_2O) C, H, N.

Ethyl 3-Chloro-3′-fluoro-4′-{(1*R*)-1-[({1-[(trifluoroacetyl)-amino]cyclopropyl}carbonyl)amino]ethyl}-1,1′-biphenyl-2-carboxylate (13c). White solid: yield 63%. ^{1}H NMR (400 MHz, $CDCl_3$) δ 1.04−1.20 (m, 5H), 1.49 (J = 7.1 Hz, 3H), 1.53−1.66 (m, 2H), 4.20 (q, J = 7.1 Hz, 2H), 5.18−5.28 (m, 1H), 6.64 (d, J = 8.3 Hz, 1H), 7.05−7.13 (m, 2H), 7.22−7.28 (m, 2H), 7.35−7.45 (m, 3H). MS m/z = 501.1 (MH^+). Anal. ($C_{23}H_{21}ClF_4N_2O_4$) C, H, N.

***N*-{(1*R*)-1-[3,3′-Difluoro-2′-(3-methyl-1,2,4-oxadiazol-5-yl)-1,1′-biphenyl-4-yl]ethyl}-1-[(trifluoroacetyl)amino]cyclopropanecarboxamide (13d).** White solid: yield 78%. ^{1}H NMR (400 MHz, CD_3OD) δ 1.01−1.29 (m, 2H), 1.45−1.51 (m, 5H), 2.36 (s, 3H), 5.27 (q, J = 7.1 Hz, 1H), 6.91−6.95 (m, 2H), 7.30−7.40 (m, 3H), 7.70−7.77 (m, 1H). HRMS Calcd for $C_{23}H_{20}F_5N_4O_3$ (M + 1): 495.1455. Found: 495.1460. Anal. ($C_{23}H_{19}F_5N_4O_3$•0.6CH2Cl2) C, H, N.

N-{(1*R*)-1-[3,3′-Difluoro-2′-(5-methyl-1,2,4-oxadiazol-3-yl)-1,1′-biphenyl-4-yl]ethyl}-1-[(trifluoroacetyl)amino]cyclopropanecarboxamide (13e). Off-white solid: yield 45%. ^{1}H NMR (400 MHz, CD_3OD) δ 1.07−1.18 (m, 2H), 1.17 (d, J = 7.0 Hz, 3H), 1.60−1.67 (m, 2H), 2.59 (s, 3H), 5.16−5.21 (m, 1H), 6.56 (d, J = 8.2 Hz, 1H), 6.94−6.99 (m, 3H), 7.15 (t, J = 7.8 Hz, 1H), 7.20−7.24 (m, 2H), 7.51−7.56 (m, 1H). MS m/z = 495.3 (MH^+). Anal. ($C_{23}H_{19}F_5N_4O_3$•0.2CH_2Cl_2) C, H, N.

***N*-{(1*R*)-1-[3,3′-Difluoro-2′-(2-methyl-2H-tetraazol-5-yl)-1,1′-biphenyl-4-yl]ethyl}-1-[(trifluoroacetyl)amino]cyclopropanecarboxamide (13f).** White solid: yield 44%. ^{1}H NMR (400 MHz, CD_3OD) δ 1.01−1.18 (m, 2H), 1.44 (d, J = 7.1 Hz, 3H), 1.49 (d, J = 3.7 Hz, 2H), 4.86 (s, 3H), 5.23 (d, J = 7.1 Hz, 1H), 6.83−6.89 (m, 2H), 7.21−7.34 (m, 3H), 7.61−7.68 (m, 1H). MS m/z = 495.32 (MH^+). Anal. ($C_{22}H_{19}F_5N_6O_2$•0.2 $CH_3CO_2C_2H_5$) C, H, N.

***N*-{(1*R*)-1-[3′-Chloro-3-fluoro-2′-(2-methyl-2*H*-tetrazol-5-yl)-biphenyl-4-yl]ethyl}-1-[(trifluoroacetyl)amino]cyclopropanecarboxamide (13g)**. White foam: yield 84%. ^{1}H NMR (400 MHz, $CDCl_3$) δ 1.04−1.15 (m, 2H), 1.42 (d, J = 7.0 Hz, 3H), 1.51−1.62 (m, 2H), 4.33 (s, 3H), 5.14 (q, J = 7.5 Hz, 1H), 6.59 (d, J = 8.2 Hz, 1H), 6.83 (m, 2H), 7.06 (t, J = 7.8 Hz, 1H), 7.33 (d, J = 7.5 Hz, 1H), 7.48−7.56 (m, 3H). HRMS Calcd for $C_{22}H_{20}ClF_4N_6O_2$ (M + 1): 511.1272. Found: 511.1276.

***N*-{(1*R*)-1-[3,3′-Difluoro-2′-(1-methyl-1H-tetraazol-5-yl)-1,1′-biphenyl-4-yl]ethyl}-1-[(trifluoroacetyl)amino]cyclopropanecarboxamide (13h).** White solid: yield 22%. ^{1}H NMR (400 MHz, CD_3OD) δ 1.04−1.19 (m, 2H), 1.43 (d, J = 7.1 Hz, 3H), 1.53−1.65 (m, 2H), 3.70 (s, 3H), 5.14−5.19 (m, 1H), 6.61 (d, J = 8.0 Hz, 1H), 6.76−6.87 (m, 2H), 7.14 (t, J = 7.8 Hz, 1H), 7.28−7.36 (m, 2H), 7.64−7.71 (m, 2H). MS m/z = 495.21 (MH^+). Anal. ($C_{22}H_{19}F_5N_6O_2$•0.1 CH_2Cl_2) C, H, N.

***N*-{(1*R*)-1-[3,3′-Difluoro-2′-(trifluoromethyl)-1,1′-biphenyl-4-yl]ethyl}-1-[(trifluoroacetyl)amino]cyclopropanecarboxamide (13i).** White solid: yield 79%. ^{1}H NMR (400 MHz, DMSO-d_6) δ 0.942−1.06 (m, 2H), 1.34−1.40 (m, 2H), 1.42 (d, J = 7.1 Hz, 3H), 5.22−5.29 (m, 1H), 7.13 (d, J = 8.1 Hz, 1H), 7.17 (d, J = 11.2 Hz, 1H), 7.25 (d, J = 7.7 Hz, 1H), 7.44 (t, J = 8.0 Hz, 1H), 7.52−7.57 (m, 1H), 7.73−7.79 (m, 1H), 8.29 (d, J = 8.1 Hz, 1H), 9.80 (s, 1H). HRMS Calcd for $C_{21}H_{16}F_8N_2O_2$ (M + 1): 418.1157. Found: 481.1173.

***N*-[(1*R*)-1-(3′-Chloro-3-fluoro-2′-propionyl-1,1′-biphenyl-4-yl)ethyl]-1-[(trifluoroacetyl)amino]cyclopropanecarboxamide (13j).** White solid: yield 12%. ^{1}H NMR (400 MHz, $CDCl_3$) δ 0.93 (t, J = 7.1 Hz, 3H), 1.07−1.20 (m, 2H), 1.49 (d, J = 7.1 Hz, 3H), 1.56−1.58 (m, 2H), 2.39 (q, J = 7.1 Hz, 2H), 5.18−5.28 (m, 1H), 6.60 (d, J = 8.1 Hz, 1H), 7.00−7.06 (m, 2H), 7.21−7.30 (m, 2H), 7.34−7.44 (m, 2H). MS m/z = 485.3 (MH^+). HRMS Calcd for $C_{23}H_{21}ClF_4N_2O_3$ (M + 1): 485.1242. Found: 485.1250.

Methyl 2-Fluoro-6-iodobenzoate (14a). To a solution of 2-fluoro-6-iodobenzoic acid (3.20 g, 12.0 mmol) in MeOH (25 mL) was added (trimethylsilyl)diazomethane (2.0 M in hexanes, 9.02 mL, 18.0 mmol). The reaction was stirred at room temperature for 2 h and then concentrated in vacuo. The residue was partitioned between CH_2Cl_2 and aqueous sodium bicarbonate. The organic layer was washed with aqueous sodium bicarbonate and brine, dried over Na_2SO_4, filtered, and concentrated. The residue was subjected to silica gel chromatography (0−5% EtOAc in hexanes) to provide **14a** (3.41 g, 100%) as a clear oil. ^{1}H NMR (300 MHz, $CDCl_3$) δ 3.98 (s, 3H), 7.10−7.15 (m, 2H), 7.65 (t, J = 4.5 Hz, 1H). MS m/z = 281.2 (MH^+).

Ethyl 2-Fluoro-6-iodobenzoate (14b). A mixture 2-fluoro-6-iodobenzoic acid (3.20 g, 12.0 mmol), potassium carbonate (1.14 g, 8.27 mmol), and iodoethane (1.76 g, 11.3 mmol) in DMF (5 mL) was stirred at room temperature for 3 h. The mixture was partitioned between EtOAc and aqueous sodium bicarbonate, and the organic extract was washed with water and brine, dried over Na_2SO_4, filtered, and concentrated. The residue was subjected to silica gel chromatography (0−5% EtOAc in hexanes) to provide **14b** (2.11 g, 95.3%) as a yellow oil. ^{1}H NMR (300 MHz, $CDCl_3$) δ 1.42 (t, J = 7.1 Hz, 3H), 4.45 (q, J = 7.1 Hz, 2H), 7.08−7.12 (m, 2H), 7.62−7.65 (m, 1H). MS m/z = 295.0 (MH^+).

5-(2-Fluoro-6-iodophenyl)-3-methyl-1,2,4-oxadiazole (14c). To a solution of 2-fluoro-6-iodobenzoic acid (15.0 g, 56.4 mmol) in CH_2Cl_2 (150 mL) containing DMF (0.1 mL) was added oxalyl chloride (9.30 g, 73.3 mmol) dropwise. The solution was stirred at room temperature for 75 min and then concentrated in vacuo. The residue was redissolved in 150 mL of CH_2Cl_2, and the solution was saturated 3 times with ammonia gas. The solution was concentrated in vacuo and dried under vacuum overnight. The residue was dissolved in *N*,*N*-dimethylacetamide dimethyl acetal (24.7 mL, 0.169 mol) and heated to 120 °C for 5 h. Additional *N*,*N*-dimethylacetamide dimethyl acetal (25 mL, 0.17 mol) was added over the course of the reaction to drive it to completion. The solution was cooled to room temperature, concentrated in vacuo, and dried under vacuum overnight. To a solution of the crude material in dioxane (57 mL) was added hydroxylamine hydrochloride (4.70 g, 67.7mmol), 5 N NaOH (13.5 mL, 67.7 mmol), and 70% acetic acid (57 mL). The mixture was stirred at 60 °C for 2 h and then at 90 °C for 3 h. The resulting solution was cooled to room temperature, diluted with EtOAc, and neutralized with aqueous sodium bicarbonate. The organic layer was washed with aqueous sodium bicarbonate and brine, dried over Na_2SO_4, filtered, and concentrated. The residue was filtered through silica gel (10% EtOAc in hexanes) to provide **14g** (8.1 g, 47%) as orange yellow crystals. ^{1}H NMR (300 MHz, $CDCl_3$) δ 2.55 (s, 3H), 7.19−7.30 (m, 2H), 7.79 (d, J = 6.3 Hz, 1H). MS m/z = 305.06 (MH^+).

5-(2-Fluoro-6-iodophenyl)-2-methyl-2H-tetraazole (14d) and 5-(2-Fluoro-6-iodophenyl)-1-methyl-1H-tetraazole (14e). A solution of commercially available (Aldrich) 2-fluoro-6-iodobenzonitrile (17.8 g, 72.2 mmol) and azidotrimethyltin (15.0 g, 72.9 mmol) in toluene (150 mL) was heated to 125 °C for 72 h. The solution was cooled to room temperature and partitioned between EtOAc and 0.5 N HCl. The organic layer was washed with water and brine, dried over Na_2SO_4, filtered, and concentrated to provide 5-(2-fluoro-6-iodophenyl)-1H-tetraazole as a white solid. A mixture of 5-(2-fluoro-6-iodophenyl)-1H-tetraazole (20.0 g, 81.0 mmol), potassium carbonate (16.1 g, 0.113 mol), and iodomethane (16.1 g, 0.113 mol) in DMF (25 mL) was stirred at room temperature for 3 h. The mixture was partitioned between EtOAc and water, and the organic extract was washed with water and brine, dried over Na_2SO_4, filtered, and concentrated. The residue was subjected to silica gel chromatography (0−10% EtOAc in hexanes) to provide **14d** (3.93 g, 26.2%) as a white solid and **14e** (9.77 g, 39.7%) as a yellow

solid. **14d**: ^{1}H NMR (300 MHz, $CDCl_3$) δ 4.48 (s, 3H), 7.18−7.24 (m, 2H), 7.77−7.80 (m, 1H). MS m/z = 305.05 (MH^+). **14e**: ^{1}H NMR (300 MHz, $CDCl_3$) δ 3.97 (s, 3H), 7.27−7.40 (m, 2H), 7.82−7.85 (m, 1H). MS m/z = 305.05 (MH^+).

3-(2-Fluoro-6-iodophenyl)-5-methyl-1,2,4-oxadiazole (14f). A mixture of 2-fluoro-6-iodobenzonitrile (12.4 g, 50.2 mmol), hydroxylamine hydrochloride (4.53 g, 65.2 mmol), and ethanol (50 mL) was stirred vigorously. To this reaction mixture was added sodium *tert*-butoxide (7.23 g, 75.3 mmol). The reaction was refluxed at 100 °C for 5 h. Additional hydroxylamine hydrochloride (4.53 g, 65.2 mmol) and sodium *tert*-butoxide (7.23 g, 75.3 mmol) were added over the course of the reaction to drive it to completion. The reaction was concentrated with ethanol under vacuum. The crude residue was dissolved in CH_2Cl_2 and washed with 1 N HCl. The aqueous layer was extracted with CH_2Cl_2 twice, basified with ammonium hydroxide slowly (pH ∼9), and re-extracted with CH_2Cl_2 3 times. The organic layers were combined, dried over Na_2SO_4, filtered, and concentrated in vacuo. The residue was subjected to silica gel chromatography (0−50% EtOAc in hexane) to afford 2-fluoro-*N*-hydroxy-6-iodobenzenecarboximidamide as a yellow oil. ^{1}H NMR (400 MHz, $CDCl_3$) δ 7.67 (t, J = 4.5 Hz, 1H), 7.12 (m, 2H), 4.78 (bs, OH). MS m/z = 281.4 (MH^+). The 2-fluoro-*N*-hydroxy-6-iodobenzenecarboximidamide (2.14 g, 7.64 mmol) was dissolved in *N*,*N*-dimethylacetamide dimethyl acetal (1.12 mL, 7.64 mmol). After 1 h and 15 min of stirring at room temperature, the reaction solution was concentrated in vacuo. The residue was subjected to silica gel chromatography (0−15% EtOAc in hexane) to provide **14f** (1.36 g, 59%) as a clear oil. ^{1}H NMR (300 MHz, $CDCl_3$) δ 7.73 (t, J = 4.3 Hz, 1H), 7.16−7.20 (m, 2H), 2.70 (s, 3H). MS m/z = 305.1 (MH^+).

Biological Methods. Receptor Binding Assays. Radioligand binding assays were performed using membranes from CHO cells that stably express the human or rat bradykinin B_1 receptors or CHO cells that express the human bradykinin B_2 receptor. For all receptor types, cells were harvested from culture flasks in PBS/1 mM EDTA and centrifuged at 1000*g* for 10 min. The cell pellets were homogenized with a polytron in ice-cold 20 mM HEPES, pH 7.4 and 1 mM EDTA (lysis buffer) and centrifuged at 50 000*g* for 20 min. The membrane pellets were rehomogenized in lysis buffer and centrifuged again at 50 000*g*, and the final pellets were resuspended at 5 mg of protein/mL in an assay buffer (20 mM HEPES, pH 7.4, 120 mM NaCl, 5 mM KCl) supplemented with 1% BSA and frozen at −80 °C.

On the day of assay, membranes were centrifuged at 14 000*g* for 5 min and resuspended to the desired protein concentration (0.2 mg/mL for typical membrane preparations) in assay buffer containing 100 nM enaliprilat, 140 μg/mL bacitracin, and 0.1% BSA. ^{3}H-des-arg^{10} leu^9 kallidin (0.2 nM) was the radioligand used for the human bradykinin B_1 receptors; ^{3}H-des-arg^{10} kallidin (1 nM) was used for the rat bradykinin B_1 receptors; and ^{3}H-bradykinin (1 nM) was used to label the human bradykinin B_2 receptor.

For all assays, compounds were diluted from DMSO stock solutions with 4 μL added to assay tubes for a final DMSO concentration of 2%. This was followed by the addition of 100 μL of the radioligand and 100 μL of the membrane suspension. Nonspecific binding for the bradykinin B_1 receptor binding assays was determined using 1 μM des-arg^{10} kallidin, while nonspecific binding for the bradykinin B_2 receptor was determined with 1 μM bradykinin. Tubes were incubated at room temperature (22 °C) for 60 min followed by filtration using a Tomtec 96-well harvesting system. Radioactivity retained by the filter was counted using a Wallac beta-plate scintillation counter.

CHO Human and Bradykinin B_1 FLIPR Protocol. CHO cells engineered to stably express the human or rat bradykinin B_1 receptor were seeded at a density of 25 000 cells per well in a 96-well plate in 200 μL of cell culture media (Iscove's modified DMEM containing 1 mg/mL G418 and 10% heat inactivated fetal calf serum). After overnight incubation at 37 °C, the cell plates were washed twice with Hank's buffered salt solution, and the cells were incubated for 60 min at 37 °C with Hank's solution containing 4 μM fluo-3 acetoxymethyl ester and 1 mM probenecid. The cells were then washed 4 times with a dye-free salt solution containing probenecid, and then 100 μL of salt solution with 1 mM probenecid was added to each well. Des-arg^{10} kallidin-induced elevation of cytosolic calcium was determined using a Fluorescence Imaging Plate Reader (FLIPR, Molecular Devices Corp., Sunnyvale, CA). All assays were conducted at 37 °C. Antagonist was added to the appropriate wells in a volume of 50 μL of Hank's solution 2 min prior to the addition of 3 nM des-arg^{10} kallidin in a 50 μL volume. Changes in cellular fluorescence due to increased cytosolic calcium ion concentrations in response to agonist were determined using an excitation wavelength of 488 nm and a 510−570 nm bandwidth emission filter. Curve fitting and IC_{50} calculations were performed using GraphPad Prism software. At least eight concentrations of antagonist were used to generate each inhibition curve.

Transepithelial Transport Assay of P-gp. A transepithelial transport study was conducted as described[27] with minor modifications. The cells were maintained in M199 media supplemented with 10% FBS. The cells at density of 5×10^4 cells/mL were plated onto a 96-well filter with 150 μL/well (pore size 3.0 μm, 0.11 cm^2 surface areas; Millipore Corp., Bedford, MA). Cells were supplemented with fresh media on the third day and used for the transport studies on the fourth day after plating. The concentrations of all test compounds were at 5 μM unless otherwise indicated. Verapamil at a 1 μM concentration was used as a marker Pgp substrate for a positive control (Sigma-Aldrich, St. Louis, MO). Hanks' Balanced Salt Solution (HBSS, Gibco-Invitrogen Corporation, Carlsbad, CA), a serum/protein free medium, was used through the experiments to eliminate any differences in protein binding among the compounds tested. Before the addition of testing compounds, the media were first replaced with HBSS media containing 1 mM HEPES to equilibrate cells into experimental conditions for 30 min. The transport experiment was then initiated by replacing the medium in each compartment with 150 μl of fresh HBSS with or without the test compound. After a 3- h incubation, 100 μL aliquots were taken from the opposite compartment as receiver samples and from the loading compartment as donor samples. The samples of the radioactive compounds were placed in scintillation vials containing 5 mL of scintillation cocktail, and the total radioactivity was measured by a liquid scintillation counter. The appearance of radioactivity in the opposite compartment was presented as a fraction of the total radioactivity added at the beginning of the experiment. Directional transport was measured in triplicate and presented as mean ± SD. The samples of unradiolabeled test compounds were analyzed by LC/MS/MS.

African Green Monkey Brain/Plasma Experiments. The test compound was prepared in 100% PEG 200 and administered iv as a bolus injection at 2 mg/kg to conscious African green monkeys (n = 2). A pre-dose sample of blood was taken as well as samples at 15 and 30 min post-dosing for determination of plasma drug concentrations. At 30 min post-dose, the animal was euthanized with pentobarbital, and the brain and spinal cord were removed. Several brain and spinal cord regions were dissected, frozen in liquid nitrogen, and stored at −70 °C until analysis by LC/MS/MS.

Rhesus LPS Model. Rhesus monkeys (male or female, 5.5−10.3 kg) were fasted overnight, placed in primate restraint chairs, and transported to the laboratory. Conscious monkeys were treated with lipopolysaccharide (LPS, 20 μg/kg of iv bolus) and allowed 2 h for hemodynamic equilibration and B_1 receptor expression. The baseline depressor response to the B_1 receptor agonist, des-Arg^{10}-kallidin (DAK, 0.3 μg/kg of iv bolus), was then measured twice with a 20 min recovery period between measurements. Pilot studies established that the depressor response to DAK remained consistent (20−23 mmHg decrease in mean arterial pressure, MAP) in this model when measured at 20 min intervals over 10 challenges. The dose−response effects of the B_1 receptor antagonist were evaluated with increasing iv bolus doses (3, 10, 30, and 100 μg/kg) given 5 min prior to each subsequent DAK administration. Following the final test of antagonist effects on DAK-induced MAP decrease, DAK challenges were repeated 4 times at 20 min intervals to investigate recovery to baseline DAK response. Blood samples were taken at 2 min after each iv dose to determine plasma concentration

of test compounds. Crossover studies were conducted with test compound versus vehicle in the same monkeys ($n = 3$), and a minimum of 2 weeks was allowed between limbs of the study.

Ex Vivo Occupancy Experiments. Transgenic hB_1 rats were dosed intravenously by infusion over a 30 min period at various doses with test compound and sacrificed. In time course studies, animals were also sacrificed at 150 and 600 min following the end of infusion. The test compound was also dosed orally, and rats were sacrificed from 0.5 to 6 h post-dose. Samples of brain and cord were quickly removed and frozen for use in the ex vivo occupancy assay, while a second set of tissue samples and a plasma samples was frozen for LCMS determination of test compound levels. For the ex vivo assay, approximately 35 mg of cord or brain was homogenized in 2000 volumes of ice-cold assay buffer (20 mM HEPES, 120 mM NaCl, 5 mM KCl, pH 7.4) and centrifuged at 75 000*g* for 10 min. The pellets were resuspended in ice-cold buffer at a concentration of 5 mg of tissue/mL and 50 μL aliquots were rapidly distributed to tubes with 0.5 mL of room-temperature buffer containing 25pM [^{35}S] 2-{(2)-1-[(3,4-dichlorophenyl)sulfonyl]-3-oxo-1,2,3,4-tetrahydroquinoxalin-2-yl}-*N*-{2-[4-(4,5-dihydro-1-imidazol-2-yl)phenyl]ethyl}acetamide. At 2, 4, 6, 8, and 10 min following membrane addition, incubations were terminated by filtration of three tubes over glass fiber filters. A parallel set of incubations performed in the presence of 100 nM unlabeled compound X was used to determine nonspecific radioligand binding at each time point. Radioactivity on the filters was determined by liquid scintillation counting, and [^{35}S] 2-{(2)-1-[(3,4-dichlorophenyl)sulfonyl]-3-oxo-1,2,3,4-tetrahydroquinoxalin-2-yl}-*N*-{2-[4-(4,5-dihydro-1-imidazol-2-yl)phenyl]ethyl}acetamide rates of association for vehicle and test compound were determined by linear regression. Receptor occupancy in a drug treated animal was calculated as: % occupancy $= (1 - (\text{slope}_{drug}/\text{slope}_{vehicle})) \times 100$. The brain and spinal cord concentrations of the test compound required to achieve 90% receptor occupancy (Occ 90%) were derived by nonlinear curve fitting using Prism software.

CFA Model of Inflammatory Pain. Male and female humanized B_1 mice and wild-type mice (8−13 weeks) were obtained from Charles River Labs. All animals were maintained in a climate-controlled room on a 12 h/12 h light/dark cycle with free access to food and water. All procedures were approved by the Institutional Animal Care and Use Committee (IACUC) at Merck and Co., Inc., West Point, PA. Baseline tactile thresholds to von Frey filaments were measured by applying a series of calibrated von Frey filaments (Stoelting, Wood Dale, IL) to the plantar aspect of the left hind paw and determining the median withdrawal threshold (grams) using the Dixon up−down method.[28] Inflammation was induced by injection of 30 μL of 50% complete Freund's adjuvant (CFA) (1:1 solution of complete and incomplete Freund's adjuvant, Sigma, St. Louis, MO) subcutaneously into the plantar surface of the hind paw. Twenty-four hours following CFA injection, mice were tested for tactile hypersensitivity using von Frey filaments. Mice were then administered either drug (6, 20, or 60 mg/kg, po) or vehicle (0.5% methyl cellulose with 10 mg/mL of malic acid, pH = 4, 10 mL/kg, po), and paw withdrawal thresholds were recorded at 60 min post-administration. Following testing at 60 min, brain and plasma samples were collected for analysis. Dose−response curves were compared by two-way repeated measures ANOVA (time × dose) with post-hoc Tukey's test (SigmaStat). Significance was defined as $p < 0.05$. CFA-induced inflammation produced a significant decrease in the paw withdrawal thresholds of both wild-type and hB_1 knock-in mice when measured 24 h after CFA injection (Figure 2). The paw withdrawal thresholds of CFA mice were unaffected by vehicle treatment. Compound **13b** dose dependently reversed the hypersensitive paw withdrawal thresholds in hB1 knock-in mice ($ED_{50} = 9.76$ mg/kg; 95% CL 6.05−15.74) but not wild-type mice (see Supporting Information).

Acknowledgment. We thank the analytical department for log *P* measurements and Joan S. Murphy for determination of high resolution mass spectra.

Supporting Information Available: Microsomal/hepatocyte stability data, CF-1 mouse data, CFA wt mouse data, and PK procedures. This material is available free of charge via the Internet at http://pubs.acs.org.

References

(1) Couture, R.; Harrisson, M.; Vianna, R. M.; Cloutier, F. Kinin receptors in pain and inflammation *Eur. J. Pharmacol.* **2001**, *429*, 161−176.

(2) Leeb-Lunberg, L. M.; Marceau, F.; Muller-Esterl, W.; Pettibone, D. J.; Zuraw, B. L. Classification of the kinin receptor family: from molecular mechanisms to pathophysiological consequences. *Pharmacol. Rev.* **2005**, *57*, 27−77.

(3) Regoli, D.; Barabé, J. Pharmacology of bradykinin and related kinins. *Pharmacol. Rev.* **1980**, *32*, 1−46.

(4) Marceau, F. Kinin B_1 receptors: a review. *Immunopharmacology* **1995**, *30*, 1−26.

(5) Mason, G. S.; Cumberbatch, M. J.; Hill, R. G.; Rupniak, N. M. J. The bradykinin B_1 receptor antagonist B9858 inhibits a nociceptive spinal reflex in rabbits. *Can. J. Physiol. Pharmacol.* **2002**, *80*, 264−268.

(6) Stewart, J. M.; Gera, L.; Chan, D. C.; Whalley, E. T.; Hanson, W. L.; Zuzack, J. S. Potent, long-acting bradykinin antagonists for a wide range of applications. *Can. J. Physiol. Pharmacol.* **1997**, *75*, 719−724.

(7) Pesquero, J. B.; Araújo, R. C.; Heppenstall, P. A.; Stucky, C. L.; Silva, J. A.; Walther, T.; Oliveira, S. M.; Pesquero, J. L.; Paiva, A. C.; Calixto, J. B.; Lewin, G. R.; Bader, M. Hypoalgesia and altered inflammatory responses in mice lacking kinin B_1 receptors. *Proc. Natl. Acad. Sci. U.S.A.* **2000**, *97*, 8140−8145.

(8) For a review, see Rupniak, N. M. J.; Longmore, J.; Hill, R. G. Elucidation of the Role of Bradykinin B_1 and B_2 Receptors in Nociception and Inflammation using Selective Antagonists and Transgenic Mice. In *Molecular Basis of Pain Induction 2000*; Wood, J. J., Ed.; Wiley Press: New York, 2000; pp 149−174.

(9) Seabrook, G. R.; Bowery, B. J.; Heavens, R.; Brown, N.; Ford, H.; Sirinathsinghi, D. J. S.; Borkowski, J. A.; Hess, J. F.; Strader, C. D.; Hill, R. G. Expression of B_1 and B_2 bradykinin receptor mRNA and their functional roles in sympathetic ganglia and sensory dorsal root ganglia neurones from wild-type and B_2 receptor knockout mice. *Neuropharmacology* **1997**, *36*, 1009−1017.

(10) Ma, Q.-P.; Hill, R. G.; Sirinathsinghji, D. J. Basal expression of bradykinin B_1 receptor in peripheral sensory ganglia in the rat. *Neuroreport* **2000**, *11*, 4003−4005.

(11) Wotherspoon, G.; Winter, J. Bradykinin B_1 receptor is constitutively expressed in the rat sensory nervous system. *Neurosci. Lett.* **2000**, *294*, 175−178.

(12) Fox, A.; Wotherspoon, G.; McNair, K.; Hudson, L.; Patel, S.; Gentry, C.; Winter, J. Regulation and function of spinal and peripheral B_1 bradykinin receptors in inflammatory mechanical hyperalgesia. *Pain* **2003**, *104*, 683−691.

(13) Conley, R. K.; Wheeldon, A.; Webb, J. K.; DiPardo, R. M.; Homnick, C. F.; Bock, M. G.; Chen, T. B.; Chang, R. S.; Pettibone, D. J.; Boyce, S. Inhibition of acute nociceptive responses in rat spinal cord by a bradykinin B_1 receptor antagonist. *Eur. J. Pharmacol.* **2005**, *527*, 44−51.

(14) For an excellent review, see: Dziadulewicz, E. K. Nonpeptide ligands for bradykinin receptors 1995−2004. *Expert. Opin. Ther. Patents* **2005**, *15*, 829−859.

(15) Kuduk, S. D.; Ng, C.; Feng, D.-M.; Wai, J. M.-C.; Chang, R. S. L.; Harrell, C. M.; Murphy, K. L.; Ransom, R. W.; Reiss, D.; Ivarsson, M.; Mason, G.; Boyce, S.; Tang, C.; Prueksaritanont, T.; Freidinger, R. M.; Pettibone, D. J.; Bock, M. G. 2,3-Diaminopyridine bradykinin B_1 receptor antagonists. *J. Med. Chem.* **2004**, *48*, 6439−6442.

(16) Feng, D. M.; Wai, J. M.; Kuduk, S. D.; Ng, C.; Murphy, K. L.; Ransom, R. W.; Reiss, D.; Chang, R. S.-L.; Harrell, C. M.; Tang, C.; Prueksaritanont, T.; Freidinger, R. M.; Pettibone, D. J.; Bock, M. G. 2,3-Diaminopyridine as a platform for designing structurally unique nonpeptide bradykinin B_1 receptor antagonists. *Bioorg. Med. Chem. Lett.* **2005**, *15*, 2385−2388.

(17) Tang, C.; Subramanian, R.; Kuo, Y.; Krymgold, S.; Liu, P.; Kuduk, S. D.; Ng, C.; Feng, D. M.; Elmore, C.; Soli, P.; Ho, J.; Bock, M. G.; Ballie, T. A.; Prueksaritanont, T. Bioactivation of 2,3-diaminopyridine-containing bradykinin B1 receptor antagonists: irrevers-

ible binding to liver microsomal proteins and formation of glutathione conjugates. *Chem. Res. Toxicol.* **2005**, *18*, 934.
(18) Wood, M. R.; Books, K. M.; Kim, J. J.; Wan, B.-L.; Murphy, K. L.; Ransom, R. W.; Chang, R. S. L.; Tang, C.; Prueksaritanont, T.; Detwiler, T. J.; Hettrick, L. A.; Landis, E. R.; Leonard, Y. M.; Krueger, J. A.; Lewis, S. D.; Pettibone, D. J.; Freidinger, R. M.; Bock, M. G. Novel bradykinin B_1 antagonists. Cyclopropylamino acid amide as a pharmacophoric replacement for 2,3-diaminopyridine. *J. Med. Chem.* **2006**, *48*, 1231−1234.
(19) Hochman, J. H.; Yamazaki, M.; Ohe, T.; Lin, J. H. Evaluation of drug interactions with P-glycoprotein in drug discovery: in vitro assessment of the potential for drug−drug interactions with P-glycoprotein. *Curr. Drug. Metab.* **2002**, *3*, 257−273.
(20) Ellman, J. A. Applications of *tert*-butanesulfinamide in the asymmetric synthesis of amines. *Pure Appl. Chem.* **2003**, **75**, 39−46.
(21) Mahar Doan, K. M.; Humphreys, J. E.; Webster, L. O.; Wring, S. A.; Shampine, L. J.; Serabjit-Singh, C. J.; Adkinson, K. K.; Polli, J. W. Passive permeability and P-glycoprotein mediated efflux differentiate central nervous system (CNS) and non-CNS marketed drugs. *J. Pharmacol. Exp. Ther.* **2002**, *303*, 1029−1037.
(22) Hochman, J.; Mei, Q.; Yamazaki, M.; Tang, C.; Prueksaritanont, T.; Bock, M.; Ha, S.; Lin, J. Role of Mechanistic Transport Studies in Lead Optimization. In *Optimizing the Drug-like Properties of Lead in Drug Discovery*; Borchardt, R. T., Kerns, E. H., Hageman, M., Thakker, D. R., Stevens, J. L., Eds.; Springer; New York, 2006; pp 28−48.
(23) Regoli, D. C.; Marceau, F.; Lavigne, J. Induction of B_1 receptors for kinins in the rabbit by a bacterial lipopolysaccharide. *Eur. J. Pharmacol.* **1981**, *71*, 105−115.
(24) Hess, J. F.; Ransom, R. W.; Zeng, Z.; Chang, R. S.; Hey, P. J.; Warren, L.; Harrell, C. M.; Murphy, K. L.; Chen, T. B.; Miller, P. J. Generation and characterization of a human bradykinin B_1 transgenic rat as a pharmacodynamic model. *J. Pharmacol. Exp. Ther.* **2004**, *310*, 488−497.
(25) Fox, A.; Kaur, S.; Li, B.; Panesar, M.; Saha, U.; Davis, C.; Dragoni, I.; Colley, S.; Ritchie, T.; Bevan, S.; Burgess, G.; McIntyre, P. Antihyperalgesic activity of a non-peptidic bradykinin B1 receptor antagonist in transgenic mice expressing the B1 receptor. *Br. J. Pharmacol.* **2005**, *144*, 889−899.
(26) Hess, F. J.; Chen, R. Z.; Hey, P.; Breese, R.; Chang, R. S.; Chen, T. B.; Bock, M. G.; Vogt, T.; Pettibone, D. J. Generation and characterization of a humanized bradykinin B1 receptor mouse. *Biol. Chem.* **2006**, *387*, 195−201.
(27) Yamazaki, M.; Neway, W. E.; Ohe, T.; Chen, I.; Rowe, J. F.; Hochman, J. H.; Chiba, M.; Lin, J. H. In vitro substrate identification studies for P-glycoprotein mediated transport: species difference and predictability of in vivo results. *J. Pharmacol. Exp. Ther.* **2001**, *296*, 723−735.
(28) Chaplan, S. R.; Bach, F. W.; Pogrel, J. W.; Chung, J. M.; Yaksh, T. L. Quantitative assessment of tactile allodynia in the rat paw. *J. Neurosci. Methods* **1994**, *53*, 55−63.

JM061094B